Materials Science & Engineering C 96 (2019) 576–582

Contents lists available at ScienceDirect

Materials Science & Engineering C

journal homepage: www.elsevier.com/locate/msec

Fabrication of gradient porous microneedle array by modified hot embossing for transdermal drug delivery

Jiyu Li[a,b,1], Yingying Zhou[c,1], Jingbo Yang[a], Rui Ye[a], Jie Gao[a], Lei Ren[a], Bin Liu[a], Liang Liang[d], Lelun Jiang[a,*]

[a] Guangdong Provincial Key Laboratory of Sensor Technology and Biomedical Instruments, School of Biomedical Engineering, Sun Yat-Sen University, Guangzhou, PR China
[b] Department of Mechanical and Biomedical Engineering, City University of Hong Kong, Hong Kong, China
[c] Department of Biomedical Engineering, Hong Kong Polytechnic University, Hong Kong, China
[d] School of Mechanical and Automotive Engineering, South China University of Technology, Guangzhou, PR China

ARTICLE INFO

Keywords:
Porous
Microneedle array
Hot-embossing
Penetration
Transdermal drug delivery
Diabetes
Insulin

ABSTRACT

A gradient porous microneedle array (GPMA) is developed for transdermal drug delivery. A modified hot embossing approach is proposed to fabricate the GPMA from poly (lactic-*co*-glycolic acid) powders within a cavity array mold under the coupling combination of gradient thermal and pressure multi-fields. The porosity of the microneedles is a gradient, and the pores are mainly distributed in the tip region. The liquid drug formulation can directly be loaded in the pores of the microneedle tips by dipping. GPMA could penetrate into the rabbit skin without breakage and the penetration force per microneedle is approximately 22 mN. The GPMA can diffuse a dry model drug, namely Rhodamine B, *in vitro* in the rabbit skin dermis. The GPMA can also effectively deliver an insulin solution *in vivo* in diabetes rats, lowering the blood glucose levels. Above all, as a dry or liquid drug carrier and a minimally invasive injector, the GPMA offers an effective alternative for transdermal drug delivery.

1. Introduction

The microneedle array (MA) is one of the most promising transdermal drug delivery systems in the pharmaceutical field [1–3]. The MA has demonstrated enhanced efficacy by delivering various therapeutic compounds across the skin barrier, with numerous advantages, such as self-administration, minimally invasive nature, first-pass-metabolism avoidance, enhanced safety and easy disposal [4,5]. The usage of the MA for transdermal drug delivery has become a major research direction in the past several decades.

At present, five different MA types have been developed for transdermal drug delivery, namely solid MA, coated MA, dissolvable/degradable MA, hollow MA, and porous MA [5–9]. Solid MA is normally employed in the “poke with patch” delivery approach, the main limitation of which is the requirement for a two-step application process, resulting in practicality issues for patients [5]. The delivery strategy of coated MA is “coat and poke” [10], and its main limitation is the restricted dosage of the drug coated on the finite microneedle surface. Dissolvable/degradable MA is prepared from a dissolvable/degradable polymer in which drugs are embedded for controlled or rapid release in the skin [10]. The delivery approach is “poke and release”, but it is impossible to load and deliver liquid drugs directly. Hollow MA can transport liquid drugs into the skin *via* its holes continuously, providing an unlimited dose of drugs. Its delivery approach is “poke and flow” [6]. The limitations of hollow MA are the complex fabrication process, potential microneedle clogging, and requirement of a syringe to inject liquid formulations [11,12]. As a single-unit drug delivery system, porous MA contains numerous randomly distributed pores in which it can load either a dry or liquid drug formulation [13]. A dry drug stored in the pores can be hydrated with the interstitial fluid, resulting in drug diffusion in the skin, while a liquid drug formulation can diffuse directly from the microneedle pores into the skin. Therefore, porous MA facilitates transdermal drug delivery by means of two major approaches: “poke and release” and “poke and flow.” Above all, the delivery approaches of these five MAs exhibit their particular merits and demerits with respect to transdermal drug delivery, and porous MA provides a flexible and multifunctional transdermal drug delivery system.

* Corresponding author.
E-mail address: jianglel@mail.sysu.edu.cn (L. Jiang).
[1] These authors contributed equally.

https://doi.org/10.1016/j.msec.2018.11.074
Received 7 February 2018; Received in revised form 25 November 2018; Accepted 28 November 2018
Available online 29 November 2018
0928-4931/

However, research on the fabrication of porous MA for transdermal drug delivery has received little attention, owing to its limitations in terms of the complex fabrication process and low mechanical strength. Several fabrication techniques have been employed to fabricate porous MA from silicon, ceramics, metal, and polymers. Chen et al. [14] and Ji et al. [15] proposed fabrication of the porous tips of silicon MA by electrochemical etching for the transdermal delivery of high molecular weight drugs. Silicon is already a brittle material and making it porous further weakens its strength, resulting in easy breakage in skin upon piercing. Maaden et al. [6] and the Luttge group [16–18] fabricated an alumina ceramic porous MA using a micro-molding technique for drug and vaccine delivery. The micro-molding technique offers the potential for up-scaling the fabrication of porous MA [10]. These alumina porous MA exhibited effective chemical and compression resistance, but were also brittle and fractured easily upon manual skin piercing [17]. Yan et al. [12] fabricated a Ti porous MA by an integrated process of wire-electrode cutting and wet etching from a porous Ti wafer for insulin injection. However, this fabrication process was costly and thus not suitable for mass production. We [13] previously proposed the fabrication of a Ti porous MA by modified metal injection molding technology for transdermal drug delivery. This porous Ti MA exhibited high mechanical strength while its biocompatibility required further investigation. Park et al. [19] ultrasonically welded poly (lactic acid) micro-particles to fabricate a porous MA for biosensing and tissue engineering. However, this polymer porous MA was fragile and unable to penetrate the skin. Liu et al. [20] fabricated a polymer porous MA by interconnecting microchannels using photopolymerization within a mold for rapid fluid transport. This porous MA exhibited sufficient penetration strength in the skin, but this research focused little on transdermal drug delivery. Overall, the cost-effective fabrication of a porous MA with high penetration strength for transdermal drug delivery remains a challenge.

In this study, we developed a novel gradient porous MA (GPMA) with high mechanical strength for skin penetration and transdermal drug delivery. The GPMA was fabricated from poly (lactic-*co*-glycolic acid) (PLGA) powders, using a modified hot embossing approach within a cavity array mold, under the coupling combination of gradient thermal and pressure multi-fields. The fabrication process was found to be simple and cost-effective. The distribution of pores in the microneedle was a gradient. The liquid drug formulation can be loaded directly and rapidly in the tip pores by dipping. The MA drug delivery efficacy is usually limited by incomplete insertion and extended period required for drug dissolution [21–23]. A drug loaded in the tips can interact directly with the interstitial fluid, thereby enhancing the utilization ratio and drug release velocity. PLGA has been used extensively in the biological field owing to its biocompatible, bioactive, and biodegradable nature. GPMA made from PLGA offers the advantage that broken microneedles left inside the skin will eventually disappear [6]. In the following sections, the GPMA fabrication process is analyzed, and the GPMA morphology and pore distribution are observed. Moreover, the penetration performance of GPMA is measured. *In vitro* diffusion of dry Rhodamine B in rabbit skin and *in vivo* delivery of an insulin solution in diabetes rats are investigated.

2. Experimental

2.1. Ethics statement

All animal procedures conducted in this work were reviewed, approved, and supervised by the Institutional Animal Care and Use Committee (IACUC), Sun Yat-sen University (Approval Number: IACUC-DD-16-0901).

2.2. Material preparation

PLGA powders (lactide/glycolide ratio of 50: 50, molecular weight range of 60–130 kD, and average particle diameter of 50 μm) were bought for the fabrication of GPMA. The Rhodamine B was purchased from Aladdin, China. Streptozotocin (Sigma, USA) and insulin (bovine pancreas, CAS: 11070-73-8, Shanghai, China) were purchased for the animal experiments. The liquid drug loading volume in the GMPA patch could be measured by a weighing method. The insulin was dissolved in dilute acid, and insulin solutions with different concentrations were prepared in advance and stored at −20 °C. Once the *in vivo* transdermal drug delivery was performed, certain volumes of insulin solutions with different concentrations were dipped in the GMPA. Samples of 0, 2.5, 5, and 10 IU insulin-loaded GPMA were prepared.

Fresh rabbit skin was prepared for the *ex-vivo* skin penetration and transdermal drug delivery. A New Zealand rabbit (male, 3 months old, 3.0 kg) was purchased from the Xinhua Experimental Animal Farm (Huadu District, Guangzhou, China). The rabbit was mercifully killed by an intravenous injection of pentobarbital. The hair was removed, and the skin was cut into squares with a size of 20 × 20 mm and thickness of 2.5 ± 0.1 mm. Sprague-Dawley (SD) rats (female, 200 ± 20 g) were provided by the Experimental Animal Center of Sun Yat-sen University, China.

2.3. Fabrication process of GPMA

A modified hot embossing method was developed for the GPMA fabrication, as illustrated in Fig. 1. The detailed fabrication procedures of the GMPA were as follows. (1) Fabrication of the cavity array mold by laser micro-machining method [24]: the cavity array molds were fabricated in one step by drilling on the top surface of 2 mm thick aluminum sheets with a laser beam, using a pulsed fiber laser engraving machine (IPG, No. YLP-1-100-20-20-CN, Germany). A 12 × 12 conical needle-shaped cavity array was fabricated on the aluminum sheet under a laser power of 20 W, laser scanning speed of 500 mm/s, and scanning number of 1500. The fabricated molds were ultrasonically cleaned for 2 h. (2) Fabrication of GPMA by modified hot embossing method: The top and bottom heating blocks were uniformly heated and maintained at the temperatures of 65 °C and 50 °C, respectively. The cavity array mold was placed on the bottom heating block. A certain amount of PLGA powder was uniformly filled in the cavities and paved on the cavity array mold surface. The top heating block was slowly compressed on the PLGA powder at a force of approximately 800 N for 30 min. Thereafter, the cavity array mold with the prepared GPMA was removed and cooled at a temperature of 35 °C for approximately 5 min. Finally, the GPMA was peeled off from the cavity array mold. (3) Plasma treatment of GPMA: the GPMA was treated with a plasma reactor (D T01, Suzhou, OPS Plasma Technology Co., Ltd). The reactor was firstly pumped at a vacuum of 5–10 Pa. Then air was injected and the pressure of reactor was maintained at 20 Pa. GPMA was plasma treated at 250 W for 10 min. The GPMA morphology was observed with an SEM (Quanta 400F, OXFORD, Holland) and digital camera (Canon, Guangzhou, China).

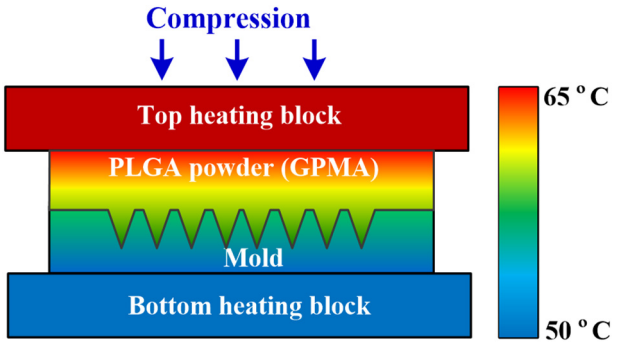

Fig. 1. Schematic of modified hot embossing setup for the GMPA fabrication.

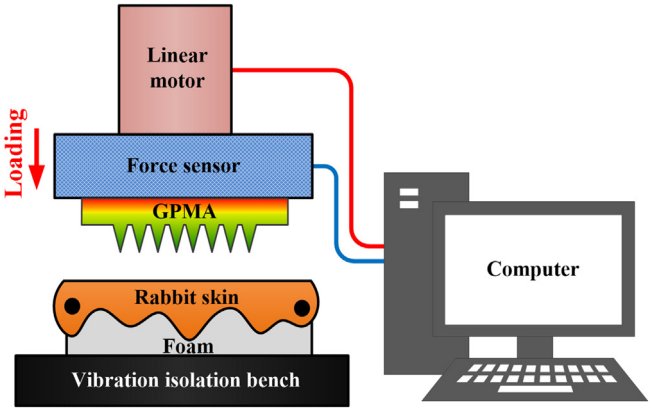

Fig. 2. Schematic of mechanical loading setup for GMPA penetration performance test.

2.4. Drug storage capacity test

Drugs can be stored in GPMA pores. The GPMA porosity was measured by the density method [25]. The drug storage capacity was investigated with a confocal laser scanning microscope (Zeiss 710, Germany). All of the GPMA microneedles were immersed in a Rhodamine B solution (1.5 ml, 0.2 wt%) for 2 min, removed and air dried for 1 h in the flow cabinet. The GPMA loaded with Rhodamine B was observed by the confocal laser scanning microscope.

2.5. Insertion test

A mechanical loading setup was developed to investigate the GPMA penetration performance, as illustrated in Fig. 2. A force sensor (Nano 17 Titanium, ATI Industrial Automation, USA) was assembled on a DC linear motor (E-861, PI, Germany). The force sensor range and resolution were 14.1 N and 2.93 mN, respectively. The loading force and displacement during the insertion process could be obtained by the force sensor and linear motor, respectively.

The fresh rabbit skin was fixed on polystyrene foam, which was used to mimic the soft tissue under the skin [26]. The GPMA was boned on a force sensor. The linear motor with GPMA was moved towards the fresh rabbit skin at a speed of 0.05 mm/s. The loading force and displacement were recorded simultaneously by self-developed software on the computer. The insertion process was stopped once the loading force reached 10 N. The insertion test was performed at a temperature of 25 °C and moisture of 90%. The punctured rabbit skin was observed with the SEM (Quanta 400F, OXFORD, Holland).

2.6. In vitro dry drug diffusion performance

The dry drug diffusion performance of the GPMA in the rabbit skin was investigated according to the following process: (1) The GPMA microneedle tips were soaked in the Rhodamine B solution (1.5 ml, 0.2 wt%) for 2 min, removed, and dried for 1 h in a flow cabinet. (2) The fresh rabbit skin was fixed on polystyrene foam. The GPMA loaded Rhodamine B was compressed on the rabbit skin under a force of approximately 5 N for 10 min. The GMPA was removed from the rabbit skin. (3) The punctured skin was observed by a microscope (BX51M, Olympus, Japan). (4) The punctured skin was embedded in a medium (O.C.T. Compound, SAKURA, Tissue-Tek ®American) to ensure optimal cutting temperature, frozen at −25 °C, and cut into 10 μm thickness slices in the vertical direction using a cryostat microtome (Leica, CM1850UV, Germany). (5) The skin slices were observed with an inverted fluorescence microscope (Eclipse Ti-E, Nikon, Japan).

2.7. In vivo transdermal insulin delivery

For this experiment, 200 ± 20 g SD rats were selected. All rats were fasted for 15 h but allowed to drink freely prior to the streptozotocin injection. The rats were intraperitoneally injected with a dose of 55 mg/kg streptozotocin in a citric acid buffer (pH 4.3) to induce type 1 diabetes. The blood glucose levels (BGLs) of the induced rats were monitored for 3 d. The rats, whose BGLs exceeded 360 mg/dL and reached a stable hyperglycemia, were used in the drug administration. The hair on the back region was shaved. Six experimental groups (n = 5 for each group) were designed for administration: healthy SD rats without treatment, diabetic SD rats treated by subcutaneous injection of insulin solution (5 IU), and diabetic SD rats treated by insulin-loaded GPMA (0, 2.5, 5, and10 IU) by dipping. The rat bloods were collected from the tail vein every hour during the 9 h administration, and the glucose concentrations were measured with a blood glucose meter (Roch®Accu-Chek, Shanghai, China).

2.8. Statistical analysis

The two groups were compared by the two-tailed student's *t*-test and the results were presented as the mean ± SD. A difference of $p < 0.05$ was regarded as statistically significant.

3. Results and discussion

3.1. GPMA fabrication and characterization

A 12 × 12 GPMA is depicted in Fig. 3(a). The two key fabrication steps of the GPMA were laser micro-machining of the cavity array mold and hot embossing of the GPMA. A conical needle-shaped cavity array is illustrated in Fig. 3(b). The micro-cavities were drilled as the focused laser beam was emitted onto the aluminum sheet surface, and the cavities were uniformly distributed on the mold. The surface of cavities was slightly rough. The distance of adjacent cavities was 1 mm, and the cavity base diameter and depth were approximately 0.45 and 0.5 mm,

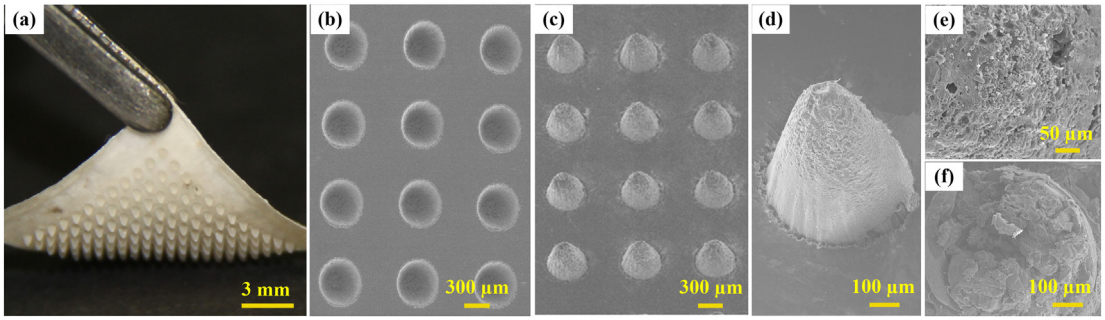

Fig. 3. (a) Digital image of GMPA. SEM images of (b) cavity array on aluminum sheet, (c) microneedle array, (d) a microneedle, (e) microneedle tip surface, and (f) cross-section of microneedle tip.

respectively. The detailed mechanism of the laser micro-machining process can be described as follows: when the focused laser beam scanned on the aluminum sheet surface, the aluminum was rapidly heated, melted, and evaporated, and then generated plasma owing to the extremely high energy density [27,28]. A laser shock was induced by the plasma expansion, removing the molten aluminum [24,29]. Finally, a conical needle-shaped cavity array was fabricated in the aluminum sheet, where the body of microneedles was formed. Laser micromachining is a simple and flexible technique for the fabrication of cavity array with various geometries.

The GPMA was fabricated using a matched cavity array mold by the modified hot embossing technique. PLGA powders were filled into the cavities and uniformly paved on the top surface of the cavity array mold. The GPMA fabrication process was accomplished using a combination of heat and pressure on the PLGA powders. The heating temperature at the interface between the top heating block and PLGA powders was approximately 65 °C, which was slightly higher than the melting point of PLGA powders. The temperature at the interface between the bottom heating block and PLGA powders was approximately 50 °C, which was below the PLGA melting point. Therefore, the temperature on the PLGA powders was gradient. Furthermore, the compression stress on the PLGA powders was gradient owing to the mechanical characteristics of the porous powder material. Therefore, under the multi-field coupling combination of temperature and compression, the PLGA powders at the GPMA substrate were completely melted together, while powders at the microneedle body were justly bonded together, finally forming the GPMA. The GPMA was peeled off from the cavity array mold as it was cooled to a temperature of 35 °C, following which it was vacuum plasma treated. The plasma treatment can increase the hydrophilic property of GPMA to enhance the absorption ability of the liquid drug [30]. Therefore, the liquid drug could be easily fulfilled into the pores under the capillary force, thus enhancing the drug loading capacity. This modified hot embossing method is simple and cost-effective.

The GPMA substrate is bendable, as illustrated in Fig. 3(a). The bendable substrate may also closely match curved human skin, maintaining a stable interface between the microneedles and skin [31]. As PLGA is one of the most promising synthetic polymers for transdermal drug delivery approved by Food and Drug Administration [32], the biocompatibility of GPMA can be strongly guaranteed. The SEM images of the fabricated GPMA are presented in Fig. 3(c–d). The cone-shaped microneedles are orderly and uniformly arranged on the substrate. The average height, base diameter, and tip diameter of the microneedles were approximately 500, 450, and 25 μm, respectively. The height was appropriate for microneedle penetration through the stratum corneum skin layer for delivering drugs [33,34]. The microneedle surface became rougher along the axial direction, as indicated in Fig. 3(d). The microneedle tip surface was the roughest owing to the existence of numerous micro pores, as shown in Fig. 3(e). A cross-section SEM image of the microneedle tip is presented in Fig. 3(f). Numerous randomly distributed pores with a variety of pore sizes (hundreds of nanometers up to several micrometers) can be found in the microneedle. The GPMA porosity was measured as approximately 20.1% according to the method previously reported [20]. The pores in the GPMA can be used to load either liquid or dry drug formulations.

3.2. Drug loading performance

The GPMA pores determine its drug storage capacity to a significant extent. The pore distribution was further investigated using a confocal laser scanning microscope. Fig. 4 shows the fluorescence microscopy images of a porous microneedle loaded with Rhodamine B. Approximately 1 μL of Rhodamine B solution was stored in the GPMA by the weighing method. The Rhodamine B solution was permeated into the pores by capillary action. A microneedle coated with dried Rhodamine B is illustrated in Fig. 4(a), and the Rhodamine B distribution in the GPMA at different slice depths is presented in Fig. 4(b). The fluorescence intensity inside the GPMA gradually decreased with the slice depth, which demonstrated that the porosity of the GPMA fabricated by means of the modified hot embossing method was a gradient. The Rhodamine B was mainly stored in the tip and rarely in the base of the microneedle. The microneedle tip within the depth range from 0 to 240 μm could be regarded as the effective drug loading region. Drugs stored in microneedle tips can be delivered into the skin more effectively, thereby increasing the drug utilization [35,36]. Microneedles are typically difficult to insert fully into skin owing to the wider needle geometry required to provide these microneedles with sufficient mechanical strength [37].

3.3. Penetration performance

The GPMA mechanical strength was weakened by making it porous, leading to breakage of porous microneedles. A MA should penetrate through the stratum corneum layer of the skin without breakage for transdermal drug delivery. The insertion force per microneedle of the GPMA during the penetration performance test is presented in Fig. 5(a–b). The insertion force gradually increased with the loading displacement due to the inherent resistance properties of rabbit skin. A small sudden drop in the insertion force could be clearly observed at point “p” in Fig. 5(a–b) as the insertion proceeded. This indicates that the GPMA compression was beyond the skin rupture limit, resulting in skin penetration. One micro-hole punctured by the GPMA in the rabbit skin can be observed, as illustrated in Fig. 5(c), which demonstrates the skin penetration. The minimum insertion force for a microneedle penetrating the stratum corneum is defined as the penetration force [38,39]. The penetration force per microneedle of the GPMA was approximately 22 mN, while the minimum energy required for skin penetration is approximately 23 μJ. The average compression force of an adult pressing the microneedles with his or her thumb is approximately 20 N [40]. Therefore, ignoring other factors, the maximum microneedle number for an adult to press the GPMA into the skin is approximately 900 in theory. The GPMA was observed following the penetration test, and it was found that the microneedles remained intact, without breakage. Therefore, the GPMA exhibits sufficient mechanical strength to penetrate the skin for transdermal drug delivery. Furthermore, the GPMA is made from biodegradable PLGA and offers the advantage that broken microneedles left inside the skin will eventually disappear [6].

3.4. Transdermal dry drug diffusion in vitro

The GPMA loaded with a dry model drug, namely Rhodamine B, at the microneedle tips is illustrated in Fig. 6(a). Approximately 0.31 μL of Rhodamine B solution was firstly absorbed in the GPMA pores and air dried. A fresh rabbit skin was punctured with this GPMA under a compression force of 5 N for 10 min, as illustrated Fig. 6(b). The red dot array on the skin surface fitted well with the arrangement of microneedles. The Rhodamine B was spread in the skin around the punctured area. Fig. 6(c) depicts the drug diffusion of a punctured skin slice. A hole with a width of approximately 80 μm and depth of approximately 60 μm created by the GPMA can be observed. The layer thickness of the stratum corneum is 10–15 μm. Therefore, the GPMA can penetrate through the stratum corneum to deliver drugs. A substantial amount of Rhodamine B was diffused around the hole tip, and the dry drug was delivered in the skin dermis layer. The possible drug diffusion process was as follows: once the drug-loaded GPMA penetrated into the skin, the drug formulation was hydrated with interstitial fluid, and hydration could occur by means of the capillary force of the pores. Evenly, the dry formulation dissolved and diffused from the tip pores into the skin [6]. Therefore, the GPMA can be employed as both a dry drug carrier and a puncher for transdermal drug delivery.

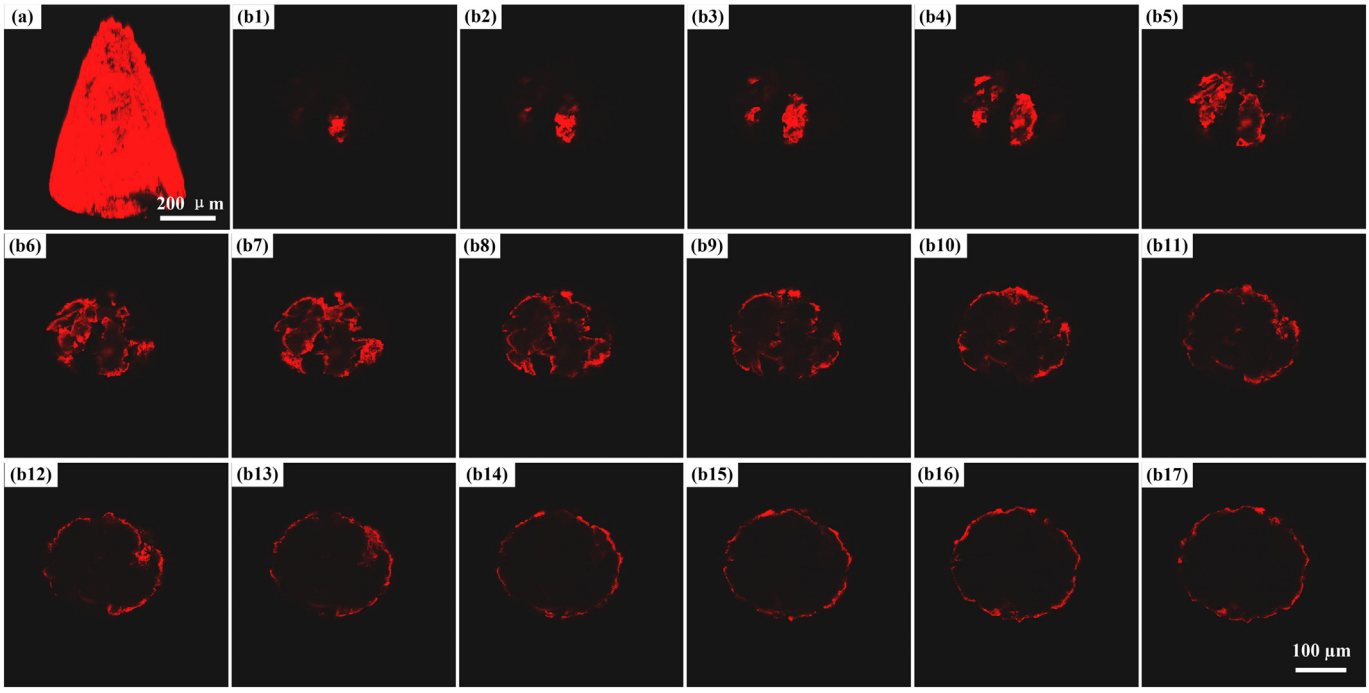

Fig. 4. Fluorescence microscopy images of porous microneedle loaded with dried Rhodamine B: (a) main body, and (b) cross-section slices at different depths with interval of 30 μm.

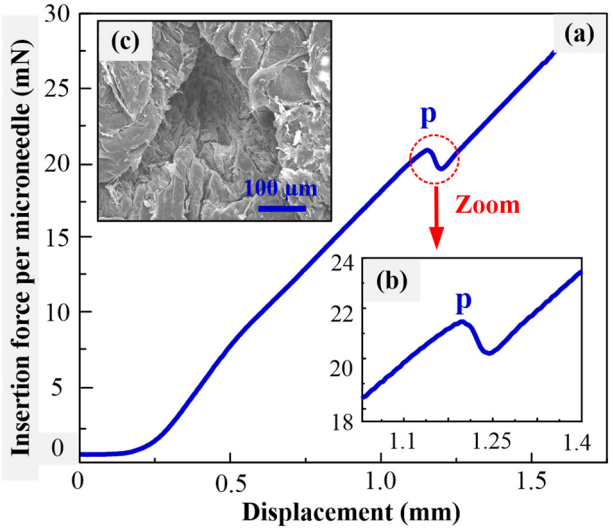

Fig. 5. (a–b) Insertion force per microneedle of GPMA with loading displacement during penetration performance test, and (c) micro hole punctured by GPMA in rabbit skin.

3.5. *In vivo* transdermal insulin delivery

Diabetes is one of the leading lethal diseases globally, and insulin is the most effective medicine for controlling BGL in type I diabetic patients [41]. In recent decades, the transdermal delivery of insulin has been regarded as an attractive alternative, owing to its easy self-administration and good patient compliance [42–45]. In this study, diabetic SD rats were selected as animal models, as illustrated in Fig. 7(a). An insulin-loaded GPMA was applied with a compression force of approximately 5 N on the rat back where the hair had been shaved off. The GPMA patch matched closely with the curved surface of the rabbit skin, as illustrated in Fig. 7(b). The skin recovery process was recorded after the GPMA was removed, as depicted in Fig. 7(c–d). The skin was rapidly recovered within 10 min, which confirmed the minimally invasive administration of the GPMA.

Fig. 7(e) presents the relationship between the BGLs over time following the administration of insulin. The healthy rats (healthy group) and diabetes rats treated with the 0 IU insulin-loaded GPMA (blank group) were used as negative controls, while the diabetes rats treated with subcutaneous injection of 5 IU insulin (SC injection group) were used as positive control. The normal blood glucose concentration of SD rats is within the range of 80 to 200 mg/dL [34,47]. The BGLs of the healthy and blank groups remained stable, at 89 ± 5 mg/dL and 361 ± 11 mg/dL, respectively. The BGL of the diabetes rats decreased rapidly from 369 ± 9 mg/dL to the minimum value of 48 ± 14 within

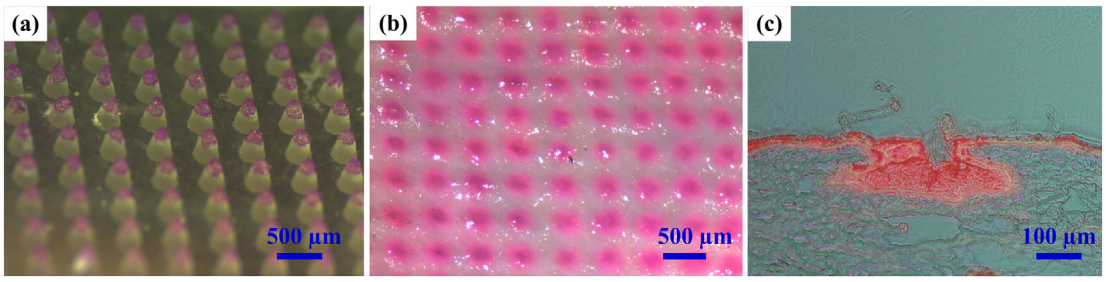

Fig. 6. (a) GPMA loaded with dried Rhodamine B at microneedle tips, (b) rabbit skin punctured by GPMA, and (c) drug diffusion image of punctured skin slice.

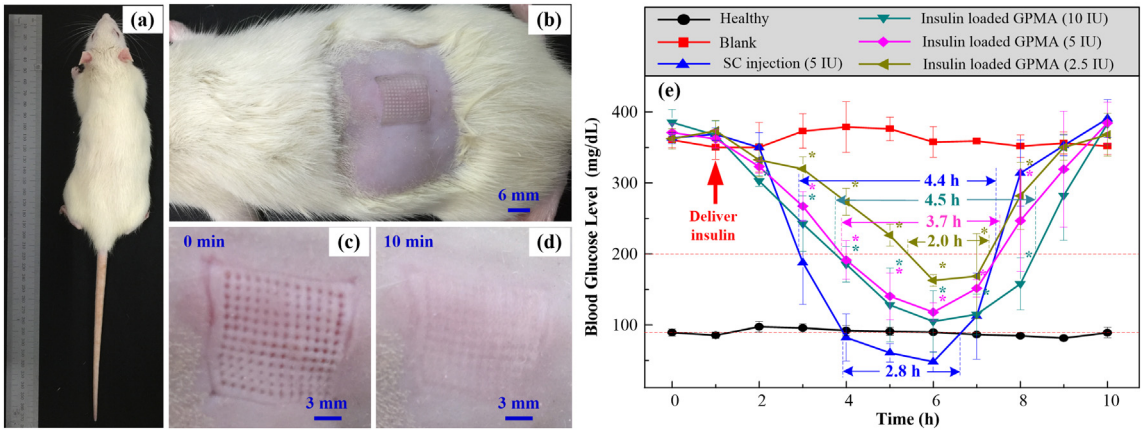

Fig. 7. Transdermal insulin delivery in diabetic rats: (a) diabetic SD rats with a weight of approximately 200 ± 20 g were selected, (b) SD rat treated with GPMA patch, (c-d) skin recovery process after removing the GPMA, and (e) BGLs in diabetic rats after transdermal administration of insulin-loaded GPMA and SC injection (n = 5).

5 h, and then rebounded to the initial level after 4 h by SC injection of 5 IU insulin. The BGLs of the SC injection group were lower than the normoglycemic concentration from 3.8 to 6.6 h, resulting in a risk of hypoglycemia [48]. Therefore, the diabetes rats treated with the SC injection were in normoglycemic concentration (80–200 mg/dL) for approximately 1.6 h.

However, following the application of 5 IU insulin-loaded GPMA, the BGLs of the diabetes rats decreased slowly and maintained a normoglycemic concentration for 3.7 h. The insulin solution stored in the microneedle pores of the GPMA was delivered into the rat skin dermis. From there, the insulin would diffuse into the blood stream and reduce the BGL [49]. The BGLs of the diabetes rats were in a normoglycemic concentration for 2 and 4.5 h with the application of 2.5 and 10 IU insulin-loaded GPMAs, respectively. A more durable effect of maintaining the BGL in normoglycemic state could be obtained by increasing the insulin-loaded dose in the GPMA, and the hypoglycemia could be effectively avoided. Furthermore, this durable effect time in the normoglycemic state when treated with the 5 IU insulin-loaded GPMA more than doubled compared to that with the 5 IU insulin SC injection. Overall, insulin delivery through the GPMA can effectively replace SC insulin delivery. In summary, GPMA can be used as both a drug carrier and an injector to deliver liquid drugs.

4. Conclusions

In this paper, a modified hot-embossing approach was proposed to fabricate a GPMA for transdermal drug delivery. A cone-shaped cavity array on the aluminum sheet was drilled by a laser beam. The GPMA was formed with the cavity array template by the modified hot embossing approach under the coupling combination of gradient thermal and pressure multi-fields. The GPMA fabrication process is proven to be simple and cost-effective. A GPMA with 12 × 12 cone-shaped gradient porous microneedles was fabricated. The GPMA exhibited sufficient mechanical strength to penetrate the skin without breakage. The minimal penetration force and energy per microneedle into rabbit skin were approximately 22 mN and 23 μJ, respectively. The pores distributed in the microneedle body formed a gradient and the GPMA porosity was approximately 20.1%. Dry or liquid drug could be loaded in the pores of the microneedles, and were mainly distributed in the tips. The GPMA could effectively deliver and diffuse a dry model drug, namely Rhodamine B, into the rabbit skin dermis. The GPMA could also deliver an insulin solution into diabetes rats. The same dose of insulin-loaded GPMA could lower the BGLs of the diabetes rats more effectively in comparison with a subcutaneous injection. In conclusion, the GPMA can be used as a dry or liquid drug carrier as well as a minimally invasive injector for transdermal drug delivery. In the future, we hope the GPMA can be used to load various liquid and dry drugs, and be applied in medical treatments.

Acknowledgments

This research was financially supported by the National Natural Science Foundation of China (Project No. 51575543), the Pearl River Nova Program of Guangzhou, China (Project No. 201806010194), and the Science and Technology Planning Project of Guangdong Province, China (Project No. 2017A030303009), and Tip-top Scientific and Technical Innovative Youth Talents of Guangdong special support program, China (2017TQ04X674).

References

[1] J.H. Park, S.O. Choi, S. Seo, Y. Bin Choy, M.R. Prausnitz, A microneedle roller for transdermal drug delivery, Eur. J. Pharm. Biopharm. 76 (2010) 282–289.
[2] C.I. Shin, S.D. Jeong, N.S. Rejinold, Y.C. Kim, Microneedles for vaccine delivery: challenges and future perspectives, Ther. Deliv. 8 (2017) 447–460.
[3] W. Yu, G. Jiang, Y. Zhang, D. Liu, B. Xu, J. Zhou, Near-infrared light triggered and separable microneedles for transdermal delivery of metformin in diabetic rats, J. Mater. Chem. B 5 (2017) 9507–9513.
[4] A. Arora, M.R. Prausnitz, S. Mitragotri, Micro-scale devices for transdermal drug delivery, Int. J. Pharm. 364 (2008) 227–236.
[5] E. Larraneta, R.E.M. Lutton, A.D. Woolfson, R.F. Donnelly, Microneedle arrays as transdermal and intradermal drug delivery systems: materials science, manufacture and commercial development, Mater. Sci. Eng. R 104 (2016) 1–32.
[6] K. van der Maaden, R. Luttge, P.J. Vos, J. Bouwstra, G. Kersten, I. Ploemen, Microneedle-based drug and vaccine delivery via nanoporous microneedle arrays, Drug Deliv. Transl. Res. 5 (2015) 397–406.
[7] K. van der Maaden, W. Jiskoot, J. Bouwstra, Microneedle technologies for (trans) dermal drug and vaccine delivery, J. Control. Release 161 (2012) 645–655.
[8] T.M. Tuan-Mahmood, M.T.C. McCrudden, B.M. Torrisi, E. McAlister, M.J. Garland, T.R.R. Singh, R.F. Donnelly, Microneedles for intradermal and transdermal drug delivery, Eur. J. Pharm. Sci. 50 (2013) 623–637.
[9] D. Liu, Y. Zhang, G. Jiang, W. Yu, B. Xu, J. Zhu, Fabrication of dissolving microneedles with thermal-responsive coating for NIR-triggered transdermal delivery of metformin on diabetic rats, ACS Biomater. Sci. Eng. (2018), https://doi.org/10.1021/acsbiomaterials.8b00159.
[10] S. Indermun, R. Luttge, Y.E. Choonara, P. Kumar, L.C. du Toit, G. Modi, V. Pillay, Current advances in the fabrication of microneedles for transdermal delivery, J. Control. Release 185 (2014) 130–138.
[11] Y.C. Kim, J.H. Park, M.R. Prausnitz, Microneedles for drug and vaccine delivery, Adv. Drug Deliv. Rev. 64 (2012) 1547–1568.
[12] X.X. Yan, J.Q. Liu, S.D. Jiang, B. Yang, C.S. Yang, Fabrication and testing of porous Ti microneedles for drug delivery, Micro Nano Lett. 8 (2013) 906–908.
[13] J.Y. Li, B. Liu, Y.Y. Zhou, Z.P. Chen, L.L. Jiang, W. Yuan, L. Liang, Fabrication of a Ti porous microneedle array by metal injection molding for transdermal drug delivery, PLoS One 12 (2017).
[14] B.T. Chen, J. Wei, F.E.H. Tay, Y.T. Wong, C. Iliescu, Silicon microneedle array with biodegradable tips for transdermal drug delivery, Microsyst. Technol. 14 (2008) 1015–1019.
[15] J. Ji, F.E.H. Tay, J.M. Miao, C. Iliescu, Microfabricated microneedle with porous tip for drug delivery, J. Micromech. Microeng. 16 (2006) 958–964.
[16] M.A. Boks, W.W.J. Unger, S. Engels, M. Ambrosini, Y. van Kooyk, R. Luttge,

Controlled release of a model vaccine by nanoporous ceramic microneedle arrays, Int. J. Pharm. 491 (2015) 375–383.
[17] S. Bystrova, R. Luttge, Micromolding for ceramic microneedle arrays, Microelectron. Eng. 88 (2011) 1681–1684.
[18] M. Verhoeven, S. Bystrova, L. Winnubst, H. Qureshi, T.D. de Gruijl, R.J. Scheper, R. Luttge, Applying ceramic nanoporous microneedle arrays as a transport interface in egg plants and an ex-vivo human skin model, Microelectron. Eng. 98 (2012) 659–662.
[19] C.S. Park, Kamath R. JH, Y.K. Yoon, M.G. Allen, M.R. Prausnitz, Polymer particle-based micromolding to fabricate novel microstructures, Biomed. Microdevices 9 (2007) 223–234.
[20] L.M. Liu, H. Kai, K. Nagamine, Y. Ogawa, M. Nishizawa, Porous polymer microneedles with interconnecting microchannels for rapid fluid transport, RSC Adv. 6 (2016) 48630–48635.
[21] H. Yang, S. Kim, I. Huh, S. Kim, S.F. Lahiji, M. Kim, H. Jung, Rapid implantation of dissolving microneedles on an electrospun pillar array, Biomaterials 64 (2015) 70–77.
[22] B.J.L.S.P. Davis, Z.H. Adams, M.G. Allen, M.R. Prausnitz, Insertion of microneedles into skin: measurement and prediction of insertion force and needle fracture force, J. Biomech. 37 (2004) 1155–1163.
[23] S.O.C.J.W. Lee, E.I. Felner, M.R. Prausnitz, Dissolving microneedle patch for transdermal delivery of human growth hormone, Small 7 (2011) 531–539.
[24] Q.L. Wang, D.D. Zhu, Y. Chen, X.D. Guo, A fabrication method of microneedle molds with controlled microstructures, Mater. Sci. Eng. C 65 (2016) 135–142.
[25] L.L. Jiang, Y. Tang, W. Zhou, L.Z. Jiang, T. Xiao, Y. Li, J.W. Gao, Design and fabrication of sintered wick for miniature cylindrical heat pipe, Trans. Nonferrous Metals Soc. China 24 (2014) 292–301.
[26] K. Chen, L. Ren, Z. Chen, C. Pan, W. Zhou, L. Jiang, Fabrication of micro-needle electrodes for bio-signal recording by a magnetization-induced self-assembly method, Sensors (Basel) 16 (2016) 1533.
[27] S.J. Xu, B. Liu, C.F. Pan, L. Ren, B.A. Tang, Q.K. Hu, L.L. Jiang, Ultrafast fabrication of micro-channels and graphite patterns on glass by nanosecond laser-induced plasma-assisted ablation (LIPAA) for electrofluidic devices, J. Mater. Process. Technol. 247 (2017) 204–213.
[28] C.F. Pan, K.Y. Chen, B. Liu, L. Ren, J.R. Wang, Q.K. Hu, L. Liang, J.H. Zhou, L.L. Jiang, Fabrication of micro-texture channel on glass by laser-induced plasma-assisted ablation and chemical corrosion for microfluidic devices, J. Mater. Process. Technol. 240 (2017) 314–323.
[29] L.L. Jiang, C.F. Pan, K.Y. Chen, J.T. Ling, W. Zhou, J.H. Zhou, L. Liang, Fiber laser carving under ice layer without laser energy attenuation, J. Mater. Process. Technol. 216 (2015) 278–286.
[30] K. Nair, B. Whiteside, C. Grant, R. Patel, C. Tuinea-Bobe, K. Norris, A. Paradkar, Investigation of plasma treatment on micro-injection moulded microneedle for drug delivery, Pharmaceutics 7 (2015) 471–485.
[31] R.X. Wang, X.M. Jiang, W. Wang, Z.H. Li, A microneedle electrode array on flexible substrate for long-term EEG monitoring, Sensors Actuators B Chem. 244 (2017) 750–758.
[32] L. Naves, C. Dhand, L. Almeida, L. Rajamani, S. Ramakrishna, G. Soares, Poly(lactic-co-glycolic) acid drug delivery systems through transdermal pathway: an overview, Prog. Biomater. 6 (2017) 1–11.
[33] Q.Y. Li, J.N. Zhang, B.Z. Chen, Q.L. Wang, X.D. Guo, A solid polymer microneedle patch pretreatment enhances the permeation of drug molecules into the skin, RSC Adv. 7 (2017) 15408–15415.
[34] W. Yu, G. Jiang, D. Liu, L. Li, H. Chen, Y. Liu, Q. Huang, Z. Tong, J. Yao, X. Kong, Fabrication of biodegradable composite microneedles based on calcium sulfate and gelatin for transdermal delivery of insulin, Mater. Sci. Eng. C 71 (2017) 725–734.
[35] D.D. Zhu, B.Z. Chen, M.C. He, X.D. Guo, Structural optimization of rapidly separating microneedles for efficient drug delivery, J. Ind. Eng. Chem. 51 (2017) 178–184.
[36] X. Xie, C. Pascual, C. Lieu, S. Oh, J. Wang, B.D. Zou, J.L. Xie, Z.H. Li, J. Xie, D.C. Yeomans, M.X. Wu, X.S. Xie, Analgesic microneedle patch for neuropathic pain therapy, ACS Nano 11 (2017) 395–406.
[37] L.Y. Chu, M.R. Prausnitz, Separable arrowhead microneedles, J. Control. Release 149 (2011) 242–249.
[38] W.K. Cho, J.A. Ankrum, D. Guo, S.A. Chester, S.Y. Yang, A. Kashyap, G.A. Campbell, R.J. Wood, R.K. Rijal, R. Karnik, R. Langer, J.M. Karp, Microstructured barbs on the North American porcupine quill enable easy tissue penetration and difficult removal, Proc. Natl. Acad. Sci. 109 (2012) 21289–21294.
[39] P. Khanna, K. Luongo, J.A. Strom, S. Bhansali, Sharpening of hollow silicon microneedles to reduce skin penetration force, J. Micromech. Microeng. 20 (2010) 045011.
[40] E. Larraneta, J. Moore, E.M. Vicente-Perez, P. Gonzalez-Vazquez, R. Lutton, A.D. Woolfson, R.F. Donnelly, A proposed model membrane and test method for microneedle insertion studies, Int. J. Pharm. 472 (2014) 65–73.
[41] Z. Chen, J. Wang, W. Sun, E. Archibong, A.R. Kahkoska, X. Zhang, Y. Lu, F.S. Ligler, J.B. Buse, Z. Gu, Synthetic beta cells for fusion-mediated dynamic insulin secretion, Nat. Chem. Biol. 14 (2018) 86–93.
[42] S. Xie, Z.J. Li, Z.Q. Yu, Microneedles for transdermal delivery of insulin, J. Drug Delivery Sci. Technol. 28 (2015) 11–17.
[43] D. Liu, B. Yu, G. Jiang, W. Yu, Y. Zhang, B. Xu, Fabrication of composite microneedles integrated with insulin-loaded $CaCO_3$ microparticles and PVP for transdermal delivery in diabetic rats, Mater. Sci. Eng. C Mater. Biol. Appl. 90 (2018) 180–188.
[44] J. Wang, Y. Ye, J. Yu, A.R. Kahkoska, X. Zhang, C. Wang, W. Sun, R.D. Corder, Z. Chen, S.A. Khan, J.B. Buse, Z. Gu, Core-shell microneedle gel for self-regulated insulin delivery, ACS Nano 12 (2018) 2466–2473.
[45] B. Xu, G. Jiang, W. Yu, D. Liu, Y. Zhang, J. Zhou, S. Sun, Y. Liu, H_2O_2-Responsive mesoporous silica nanoparticles integrated with microneedle patches for the glucose-monitored transdermal delivery of insulin, J. Mater. Chem. B 5 (2017) 8200–8208.
[47] W.J. Yu, G.H. Jiang, Y. Zhang, D.P. Liu, B. Xu, J.Y. Zhou, Polymer microneedles fabricated from alginate and hyaluronate for transdermal delivery of insulin, Mater. Sci. Eng. C 80 (2017) 187–196.
[48] Y. Ohkubo, H. Kishikawa, E. Araki, T. Miyata, S. Isami, S. Motoyoshi, Y. Kojima, N. Furuyoshi, M. Shichiri, Intensive insulin therapy prevents the progression of diabetic microvascular complications in Japanese patients with non-insulin-dependent diabetes mellitus: a randomized prospective 6-year study, Diabetes Res. Clin. Pract. 28 (1995) 103–117.
[49] K.B. Vinayakumar, P.G. Kulkarni, M.M. Nayak, N.S. Dinesh, G.M. Hegde, S.G. Ramachandra, K. Rajanna, A hollow stainless steel microneedle array to deliver insulin to a diabetic rat, J. Micromech. Microeng. 26 (2016).